Available online at www.sciencedirect.com
ScienceDirect
Trans. Nonferrous Met. Soc. China 25(2015) 122−128
Transactions of Nonferrous Metals Society of China
www.tnmsc.cn

Magnetostriction and microstructure of melt-spun $Fe_{77}Ga_{23}$ ribbons prepared with different wheel velocities

Hao LIU[1], Hai-ou WANG[1], Meng-xiong CAO[1], Wei-shi TAN[1],
Yang-guang SHI[2], Feng XU[3], Quan-jie JIA[4] , Yu-ying HUANG[5]

1. Key Laboratory of Soft Chemistry and Functional Materials, Ministry of Education, Department of Applied Physics, Nanjing University of Science and Technology, Nanjing 210094, China;
2. Department of Applied Physics, Nanjing University of Aeronautics and Astronautics, Nanjing 211106, China;
3. School of Materials Science and Engineering, Nanjing University of Science and Technology, Nanjing 210094, China;
4. Institute of High Energy Physics, Chinese Academy of Sciences, Beijing 100039, China;
5. Shanghai Institute of Applied Physics, Chinese Academy of Sciences, Shanghai 201800, China

Received 13 July 2014; accepted 28 November 2014

Abstract: A set of stacked ribbons with the composition of $Fe_{77}Ga_{23}$ were prepared with different wheel velocities of 7 m/s, 12.5 m/s and 25 m/s (named as S_7, $S_{12.5}$ and S_{25}, respectively). High resolution X-ray diffraction patterns of these ribbons show that all the ribbons present the disordered A_2 structure, whereas an additional modified-DO_3 phase is detected in $S_{12.5}$ and S_{25}. S_{25} has stronger (100) texture than other two samples. Ga K-edge extended X-ray absorption fine structure results indicate that both bond distance and the number of Ga atoms in the second neighbor shell around Ga decrease with increasing wheel velocity. No Ga cluster is detected in the studied ribbons. A short-range ordering Ga-rich phase and large local strain have no obvious influence on magnetostriction of S_7. It is believed that both the (100) texture and the additional modified-DO_3 phase play a positive role in magnetostrictive properties of $Fe_{77}Ga_{23}$ ribbons.

Key words: magnetostriction; texture; modified-DO_3 phase; melt-spun $Fe_{77}Ga_{23}$ ribbon

1 Introduction

Fe−Ga alloy (Galfenol) is a new type of magnetostriction material, which has received extensive attention because giant magnetostriction of $Fe_{100-x}Ga_x$ alloys ($15<x<27$) offers potential application for future generation of sensors and actuators [1]. [100] oriented $Fe_{100-x}Ga_x$ single crystal with $13\le x\le 23$ can exhibit magnetostriction of 400×10^{-6} [2]. However, the high cost of single crystal drives people to find other novel synthetic method. Thin melt-spun ribbon minimizes ac-eddy current losses and will be well suitable for working at high frequency. In addition, thin melt-spun ribbon has probable higher magnetostriction than single crystal. For example, the saturation magnetostriction of Fe−Ga melt-spun ribbon was reported to reach the values as high as 2000×10^{-6}, if the magnetostriction was measured along the ribbon length applying the magnetic field perpendicular to the ribbon plane using strain-gauge method [3,4]. To explain the origin of giant magnetostriction in Fe−Ga alloys, WU [5] proposed a model and suggested a tetragonal "modified-DO_3 (or B_2-like)" structure from first principles calculation. Subsequently, CULLEN et al [6] modeled the behavior of the magnetocrystalline anisotropy of Fe−Ga alloys and concluded that such a "modified-DO_3" structure could be formed by Ga atom pairs distributed along [001] direction. In 2003, LOGRASSO et al [7] found an abnormal diffraction peak around 44° in the X-ray diffraction (XRD) pattern of (100) and (111)-oriented single crystal, and using the model based on the modified-DO_3 phase, they theoretically explained this abnormal diffraction peak perfectly. In recent work, a diffraction peak split in XRD pattern of A_2 matrix has been reported and attributed to the occurrence of modified- DO_3 phase [8−10]. But these conclusions were controversial because this split of XRD peak could result

Foundation item: Projects (11079022, 51271093, 10904071, U1332106) supported by the National Natural Science Foundation of China
Corresponding author: Wei-shi TAN; Tel: +86-25-84303380; E-mail: tanweishi@njust.edu.cn
DOI: 10.1016/S1003-6326(15)63586-5

from not only the modified-DO_3 phase but also DO_3 and B_2 phase. In addition, the superlattice reflections were very weak due to little difference between the atomic scattering factor of Fe and Ga. In fact, there are several difficulties in phase identification using normal XRD due to limitation of instrument resolution and the feature of samples. Therefore, there were no sufficient experimental data to evidence the existence of modified-DO_3 phase in Fe−Ga alloy. Furthermore, the Ga-cluster model was proposed to explain the giant magneto-striction in Fe−Ga alloys [11], and this model was excluded by PASCARELLI et al [12]. Consequently, more researches especially on the microstructure of Fe−Ga alloy are needed to elucidate the origin of giant magnetostrction in melt-spun ribbons.

Previous reports indicated that the magnetostriction of Fe−Ga ribbons with the same composition was different. In this work, in order to study the difference between the magnetostriction of Fe−Ga ribbons with the same composition and origin of giant magnetostriction in Fe−Ga ribbons, a set of ribbons with the nominal composition of $Fe_{77}Ga_{23}$ were prepared with different wheel velocities and thus with different cooling rates. High resolution X-ray diffraction (HRXRD) was performed using synchrotron radiation facility to observe the weak superlattice reflections in XRD patterns. As a supplement of HRXRD, extended X-ray absorption fine structure (EXAFS) was utilized to characterize the local structure of ribbons. Then the influence of wheel velocity on the microstructure and the magnetostrictive properties of Fe−Ga ribbon was further discussed.

2 Experimental

The ingot with nominal composition of $Fe_{77}Ga_{23}$ was prepared using high purity Fe and Ga (99.999%) in an induction furnace under argon atmosphere. It was re-melted 5 times to make ingot homogeneous. The as-cast ingot was crushed into small pieces of about 5 g, which were then melt-spun to ribbons using linear velocities of 7 m/s, 12.5 m/s and 25 m/s. Hereafter these three ribbons were named as S_7, $S_{12.5}$ and S_{25}, respectively. The as-spun ribbons are with the width of 2.5 mm and the thickness of 30−80 μm while the wheel velocity increases from 7 m/s to 25 m/s.

Optical micrographs of samples S_7, $S_{12.5}$ and S_{25} were obtained by optical microscopy. HRXRD patterns and rocking curve of (200) plane were measured at beam line BL14B of Shanghai Synchrotron Radiation Facility (SSRF) with wavelength of 0.12438 nm. Transmission extended X-ray absorption fine structure spectroscopy (EXAFS) measurements were performed at beam line 1W2B of Beijing Synchrotron Radiation Facility (BSRF) using double crystal Si (111) monochromator. The ribbons were polished to be about 30 μm thickness to provide one unit absorption jump at the Ga K-edge. The stacked samples were made by gluing about 20 ribbons together, and sticking on standard strain gauges to measure the magnetostriction in the corresponding directions applying the magnetic field along the normal direction of the ribbons. Magnetization of ribbons was measured using vibrating sample magnetometer (VSM).

3 Results and discussion

3.1 Microstructural characterization of $Fe_{77}Ga_{23}$ ribbons

3.1.1 Metallographic analysis of $Fe_{77}Ga_{23}$ ribbons

The micrographs of the cross section of samples S_7, $S_{12.5}$ and S_{25} are shown in Fig. 1. The microstructure of ribbon shows columnar grains in the solidification direction. The columnar grains originated from large temperature gradient appear along the normal direction of the ribbon during the quenching procedure [13]. This columnar grains were also observed in bulk Fe−Ga alloy prepared by copper mold casting and the Fe−Ga rods [14,15]. As the wheel velocity is increased from 7 to 12.5 m/s, the cooling rate increases and therefore the columnar grains are elongated and almost crossed the whole section due to the larger temperature gradient. When the cooling rate and the driving force of solidification are enhanced for the case of wheel velocity of 25 m/s, the thermal diffusion replaces the solute diffusion in the leading role of grain growth. Therefore, the crystal nucleus grows rapidly and meets to form large grains. This result indicates that the increase of wheel velocity induces higher cooling rate and improves the crystallization quality significantly. A little dark dots are detected in samples $S_{12.5}$ and S_{25}.

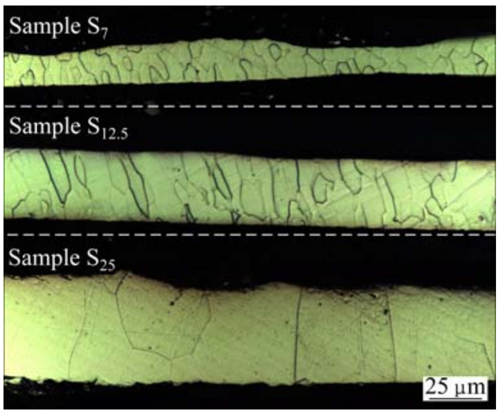

Fig. 1 Optical micrographs of samples S_7, $S_{12.5}$ and S_{25}

3.1.2 HRXRD analysis of $Fe_{77}Ga_{23}$ ribbons

The HRXRD patterns shown in Fig. 2(a) demonstrate that the disordered A_2 phase is the main phase in all samples. As shown in the inset of Fig. 2(a), split of (200) peak is detected in sample $S_{12.5}$ which probably results from an ordered DO_3 or modified-DO_3 phase. Comparing with the standard XRD pattern of A_2 phase, it is found that only two main diffraction peaks exist while a weak diffraction peak at 24.6° emerges and (211) peak at 63° disappears in sample S_{25}. High intensity of (200) peak indicates that there is an obvious (100) texture in S_{25} sample. Rocking curve of (200) peak in S_{25} sample is measured and presented in Fig. 2(b). Two peaks in Fig. 2(b) may relate to the (100) texture of A_2 phase and another ordered phase. In addition, the [100] orientation is approximately parallel to the ribbon normal concluding from the rocking curve. As known to all, grains orient randomly in ideal polycrystal and all the diffraction peaks exist in the XRD pattern, therefore the rocking curve of the lattice plane is shown as one straight line parallel to the ω-axis. For the case of ideal single crystal, the whole crystal could be seen as one large grain and diffraction peaks should be from (*hkl*) or (*nh*, *nk*, *nl*) lattice plane, therefore, the rocking curve of (*hkl*) or (*nh*, *nk*, *nl*) will be one narrow peak with full width at half maximum (FWHM) of about several arc seconds. The disappearance of (211) diffraction peak in sample S_{25} and the shape of the rocking curve indicate that the (100) texture is enhanced by increasing the cooling rate. The split of left-side peak in the rocking curve should result from the mosaic structure with small deviation angle.

3.1.3 EXAFS analysis of $Fe_{77}Ga_{23}$ ribbons

In order to probe the local environment of the ribbons and reveal the origin for the split of (200) diffraction peak and appearance of the diffraction peak around 24.6° in HRXRD pattern, Ga K-edge EXAFS of all the ribbons were measured. The Athena and Artemis programs based on the IFEFFIT library of numerical XAFS algorithms were applied [16]. The EXAFS oscillations were extracted from the experimental data using standard procedures [17]. The pre-edge background was subtracted with a linear function while R_{bkg} parameter was equal to 0.12 nm. The normalized $\mu(E)$ is shown in Fig. 3(a). It is found that behind the absorption edge, there is an obvious difference between the shape and amplitude of the normalized $\mu(E)$ curve of these three samples. Especially for the sample S_7, its first oscillation in normalized $\mu(E)$ is weaker than that in samples $S_{12.5}$ and S_{25}. The k^2 weighted $\chi(k)$ data, to enhance the oscillations at higher k, were Fourier transformed (FT), and the FT was calculated using the Hanning filtering function. Besides the amplitude damping factors S_0^2, the intensity of FT peaks reflect both the coordination of ions of those radial distances

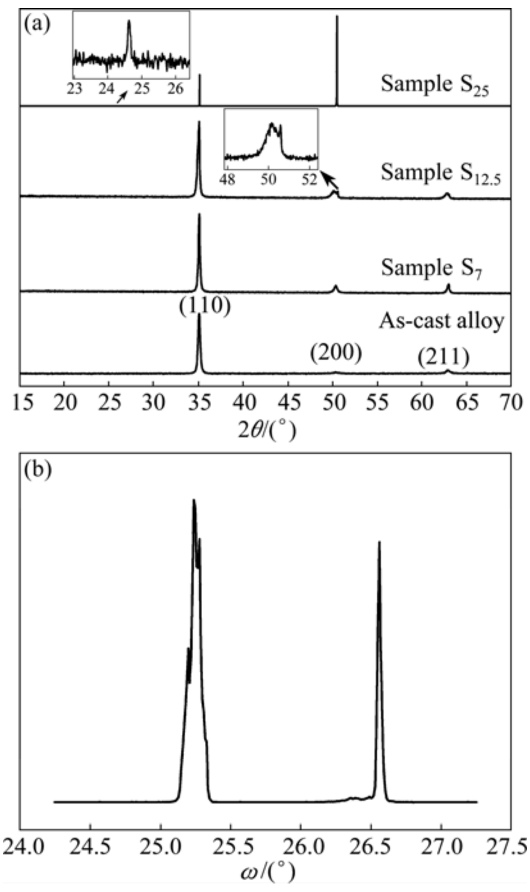

Fig. 2 HRXRD patterns of samples S_7, $S_{12.5}$ and S_{25} (a) and rocking curve of (200) diffraction peak of sample S_{25} (b)

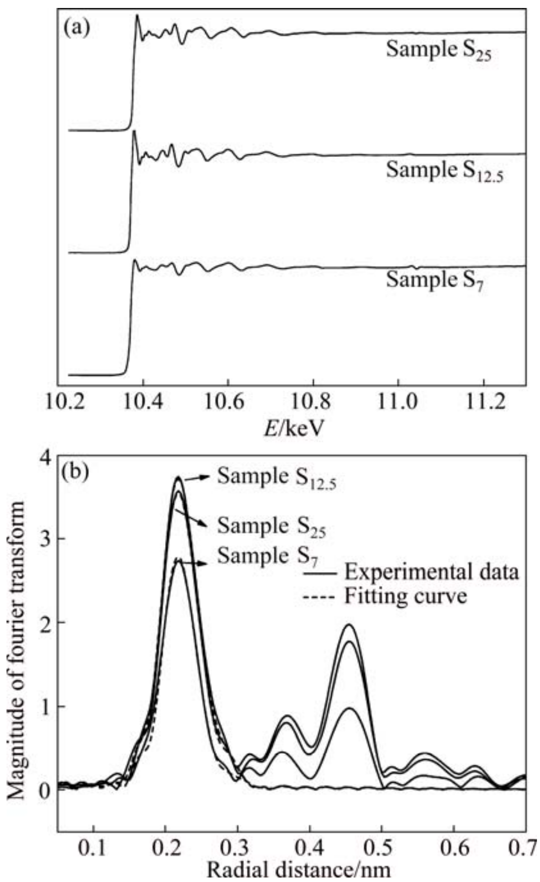

Fig. 3 Nomalized $\mu(E)$ curve of Ga K-edge EXAFS of samples S_7, $S_{12.5}$ and S_{25} (a) and experimental and fitting curves of Ga K-edge EXAFS in R space (b)

and the Debye−Waller factor (disorder factor). HRXRD patterns of ribbons imply that all the samples maintain BCC matrix, so the numbers of atoms in the first and second neighbor shells around Ga in all the ribbons are 8 and 6, respectively. In addition, the difference between the shapes of FT peaks may be from the proportion of Fe and Ga atoms in the coordination shells, thus the FT peaks shown in Fig. 3(b) are believed to correspond with S_0^2, atomic disorder and the proportion of Fe and Ga atoms. The fitting is performed in the range from 20 $\text{nm}^{-1}<k<130$ nm^{-1}. The fitting range in R space is from 0.1 nm to 0.3 nm which covers two neighbor shells, but only one FT peak can be observed, therefore special fitting procedure must be used to distinct these two shells.

To make the fitting results more credible, Ga K-edge spectra of three samples in R space were fitted simultaneously. The number of atoms in the first and second neighbor shells around Ga in all the ribbons was set as 8 and 6, respectively. The $E_{0-\text{Fe}}$ and $E_{0-\text{Ga}}$ were fixed to 1.8 eV and 7.8 eV, respectively. Ga atoms in the first neighbor shell of Ga atom were tested by substituting one Ga for one Fe. Unfortunately, the reduced χ_v^2 increases sharply when Fe atom is substituted by Ga atoms in the first shell. Therefore it should be concluded that there is no Ga atom in the first shell of studied ribbons. This result is consistent with that for the $Fe_{80}Ga_{20}$ ribbon reported by PASCARELLI et al [12]. They concluded that the absence of first shell Ga atoms resulted from the mechanism for the distorted crystal to minimize the elastic energy. The absence of Ga atoms in the first shell implied that Ga clusters did not exist in these studied ribbons. Thus the proportion of Ga in the second neighbor shell around Ga atoms is only fitted. The S_0^2 of samples S_7, $S_{12.5}$ and S_{25} are fitted to be 0.5, 0.71 and 0.68, respectively. Figure 3(b) shows the results of fitting. The Structural parameters obtained from fitting are listed in Table 1. From these structural parameters, it can be concluded that as the wheel velocity increases, the number of Ga atoms in the second neighbor shell around Ga atom decreases and the bond distance shrinks a little. Since the substitution of Fe by Ga introduces local strain, the interatomic second shell Ga−Ga distance (~0.3 nm) is larger than the corresponding Fe−Fe distance of the host lattice (~0.288 nm). In sample S_7, the interatomic second shell Ga−Ga distance reaches 0.307 nm, which is larger than that of samples $S_{12.5}$ and S_{25} (0.304 nm). The bond distance change reaches 6% and indicates that a large local strain emerges in sample S_7. The number of Ga atom in the second shell of samples $S_{12.5}$ and S_{25} is approximately equal to 2 while this number for sample S_7 is approximately equal to 3. In HRXRD pattern of sample S_7, only three diffraction peaks of A_2 phase are observed, which implies that the Ga atoms in the grain lattice of sample S_7 are distributed randomly, thus the number of Ga in the second shell should be the average value of 1.38, but are about 3 Ga atoms in the second shell in sample S_7. This phenomenon could result from a short-range ordering (SRO) Ga-rich phase. That is also the reason why no superlattice reflection is observed in the HRXRD pattern of sample S_7. The SRO phase exists in the form of nanoscale precipitate, so it could not be observed by optical microscopy in Fig. 1 [18]. The number of Ga atoms in the second shell of samples $S_{12.5}$ and S_{25}, as shown in Table 1, indicates that both the appearance of peak at 24.6° in HRXRD pattern of S_{25} and the split of (200) peak in HRXRD pattern of $S_{12.5}$ are related to a long-range ordering (LRO) modified-DO_3 phase [7]. In modified-DO_3 phase, there are 2 Ga atoms in the second neighbor coordination shell. The analysis above shows that the modified-DO_3 phase is observed in samples $S_{12.5}$ and S_{25}. It is believed that the modified-DO_3 phase exists in the form of dark dot-like phase which is shown in Fig. 1.

3.2 Physical properties of $Fe_{77}Ga_{23}$ ribbons

3.2.1 Magnetic properties characterization

The magnetic loops of sample S_{25} are shown in Fig. 4(a). The magnetic field is applied along the length direction and normal direction of ribbon, respectively. Magnetization quickly saturates for the magnetic field applied along the length direction. It indicates that there is strong magnetic anisotropy in sample S_{25}. The magnetic anisotropy includes two parts: the shape anisotropy of ribbons and the magnetocrystalline anisotropy due to texture. From HRXRD patterns and rocking curve, it is known that sample S_{25} is of strong (100) texture and the [100] direction orients along the normal direction of the ribbons. Because the [100] orientation is the easy magnetic axis in Fe−Ga alloys [19], it is believed that the magnetic anisotropy in melt-spun ribbons is mainly from the shape anisotropy

Table 1 Structural parameters obtained from fitting of Ga K-edge EXAFS

Sample	$R^{\text{I}}_{\text{GaFe}}$/nm	$R^{\text{II}}_{\text{GaFe}}$/nm	$R^{\text{II}}_{\text{GaGa}}$/nm	$N^{\text{II}}_{\text{GaGa}}$	$(\sigma^2)^{\text{I}}_{\text{GaFe}}/10^{-5}\text{nm}^2$	$(\sigma^2)^{\text{II}}_{\text{GaFe}}/10^{-5}\text{nm}^2$	$(\sigma^2)^{\text{II}}_{\text{GaGa}}/10^{-5}\text{nm}^2$
S_7	0.2505±0.0003	0.2893±0.0004	0.307±0.002	2.9±0.5	3.3 ±0.6	3.3 ±0.6	9±4
$S_{12.5}$	0.2499±0.0003	0.2886±0.0004	0.304±0.002	2.0±0.4	4.8±0.5	4.8±0.5	6±2
S_{25}	0.2496±0.0003	0.2882±0.0004	0.304±0.002	1.9±0.4	4.7±0.6	4.7±0.6	6±2

R, N and σ present bond distance, coordination numbers and Debye-Waller factor, respectively. The uncertainties are also shown (superscript I and II represent the first and second shell, respectively)

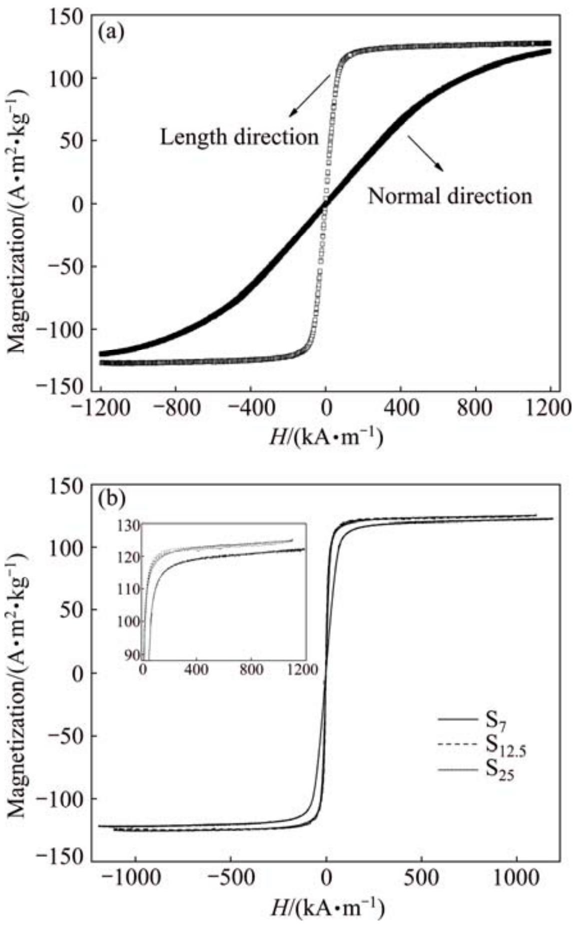

Fig. 4 Magnetization of sample S_{25} when magnetic field is applied along length direction and along normal direction (a) and magnetization of ribbons prepared with different wheel velocities when magnetic field is applied along length direction (b)

which forces magnetic moments staying within the ribbon plane, resulting in strong demagnetizing field along the ribbon normal direction. Similar phenomena have been reported in Refs. [4,20].

Magnetization curves of $Fe_{77}Ga_{23}$ ribbons with different wheel velocities are demonstrated in Fig. 4(b). In the measurement, magnetic field is applied along the length direction of ribbons. It could be observed that the saturation magnetization of sample S_7 is 122.2 A·m^2/kg. As the wheel velocity increases, the saturation magnetization increases to be 124.8 A·m^2/kg. This result indicates that the SRO Ga-rich phase with more non-magnetic atoms is of lower saturation magnetization than that of modified-DO_3 phase. Therefore, the appearance of SRO Ga-rich phase in sample S_7 results in lower saturation magnetization as compared with that in $S_{12.5}$ and S_{25} ribbons.

3.2.2 Magnetostrictive properties characterization

Figure 5 shows the magnetostriction measured from stacked ribbon samples S_7, $S_{12.5}$ and S_{25}. As can be seen, the magnetostriction increases slowly in the low field region, then increases dramatically and saturated. The saturated magnetostrictions of samples S_7, $S_{12.5}$ and S_{25} reach -109×10^{-6}, -149×10^{-6} and -235×10^{-6}, respectively.

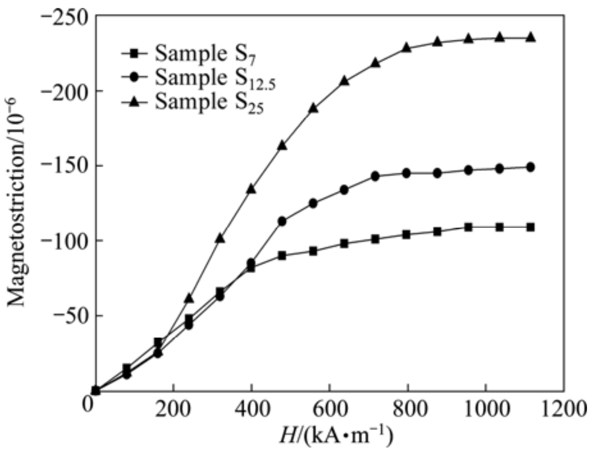

Fig. 5 Magnetostriction along length direction of melt-spun $Fe_{77}Ga_{23}$ ribbons prepared with different wheel velocities (Magnetic field was applied along normal direction of ribbons)

3.3 Discussion

In the process of melt-spinning, large temperature gradient appear and grains grow along the direction of the temperature gradient. The cooling rate is relatively lower with lower wheel velocity and Ga-rich phase produced by metastable liquid separation has sufficient time to coagulate. With increasing wheel velocity, the cooling rate increases by one order magnitude and the coagulation of Ga-rich phase is suppressed [21]. At the same time, the higher cooling rate improves the degree of order, Ga atoms distribute along [100] orientation, i.e., the direction of the temperature gradient, thus LRO modified-DO_3 phase appears in samples $S_{12.5}$ and S_{25}. However, no nearest neighbor Ga−Ga atom pairs was detected in these studied ribbons. The absence of Ga−Ga atom pairs results from the mechanism for the distorted crystal to minimize the elastic energy. In modified-DO_3 phase, Ga−Ga atom pairs locate at the body-centered positions along [100] directions. The Ga−Ga atom pairs can soften the modulus of elasticity and increase the energy density and, therefore, enhance the magnetostriction [22].

Compared the HRXRD patterns of the as-cast alloy with the ribbons shown in Fig. 2(a), it is found that all the ribbons exhibit (100) texture, but the (100) texture dose not vary linearly with the increasing of wheel velocity. The sudden increase of the intensity of (100) diffraction peak in sample S_{25} indicates that there probably exists a critical cooling rate to produce strong (100) texture. Rocking curve and micrograph of sample S_{25} indicate that an appropriate wheel velocity and proper cooling rate could produce a good substitute of the single crystal. The structural anisotropy in the ribbons induces magnetic anisotropy, as shown in Fig. 4(a).

From Figs. 1, 4(b) and 5, an interesting phenomenon is found. The saturation magnetization and saturation magnetostriction increases with the increase of grain size. The enhancement of saturation magnetization is believed to result from the emergence of SRO Ga-rich phase. And the saturation magnetostriction is related to the differences in preferred orientation. The saturation magnetostriction of polycrystalline material depends both on the magnetostrictive properties of the individual crystals and on the arrangement way, i.e., on the presence or absence of preferred domain or grain orientation [23]. Larger grain size and stronger grain orientation will be helpful to obtaining larger magnetostriction.

From the discussion above, it is believed that there are two main factors affecting the magnetostrictive properties of $F_{77}Ga_{23}$ ribbons, i.e., modified-DO_3 phase and (100) texture. The sample S_{25} has the largest magnetostrction of -235×10^{-6} due to modified DO_3 phase and strongest (100) texture. On the other hand, although modified-DO_3 phase is detected in sample $S_{12.5}$, the magnetostriction of this ribbon is smaller than that of sample S_{25} due to the lack of strong (100) texture. In sample S_7, the Ga-rich phase does not play a positive role in enhancement of magnetostriction.

4 Conclusions

1) The microstructure of $Fe_{77}Ga_{23}$ ribbons prepared by different wheel velocities was characterized using HRXRD and EXAFS. No Ga cluster was detected in the studied ribbons. A SRO Ga-rich phase and large (6%) local strain were detected in sample S_7, but they have no remarkable influence on the magnetostrictive properties of Fe−Ga ribbons.

2) As the wheel velocity increases, modified-DO_3 phase appears in samples $S_{12.5}$ and S_{25} due to high cooling rate. In modified-DO_3 phase, Ga−Ga atom pairs locate at the body-centered positions along [100] direction. Stronger (100) texture is found in sample S_{25}, and the [100] orientation is parallel to the ribbon normal direction.

3) Both the modified-DO_3 phase and (100) oriented texture play a positive role in the magnetostrictive properties of $Fe_{77}Ga_{23}$ ribbons. The magnetostriction of -235×10^{-6} is obtained in sample S_{25}.

Acknowledgement

We acknowledge Shanghai Synchrotron Radiation Facility and Beijing Synchrotron Radiation Facility for providing the beam time.

References

[1] ENGDAHL G. Handbook of giant magnetostrictive materials [M]. San Diego: Academic Press, 1999.

[2] CLARK A E, HATHAWAY K B, WUN-FOGLE M, RESTORFF J B, LOGRASSO T A, KEPPENS V M, PETCULESCU G, TAYLOR R A. Extraordinary magnetoelasticity and lattice softening in BCC Fe−Ga alloys [J]. Journal of Applied Physics, 2003, 93(10): 8621−8623.

[3] ZHANG M C, JIANG H L, GAO X X, ZHU J, ZHOU S Z. Magnetostriction and microstructure of the melt-spun $Fe_{83}Ga_{17}$ alloy [J]. Journal of Applied Physics, 2006, 99(2): 023903-1−023903-3.

[4] LIU G D, LIU L B, LIU Z H, ZHANG M, CHEN J L, LI J Q, WU G H, LI Y X, QU J P, CHIN T S. Giant magnetostriction on $Fe_{85}Ga_{15}$ stacked ribbon samples [J]. Applied Physics Letters, 2004, 84(12): 2124−2126.

[5] WU R. Origin of large magnetostriction in FeGa alloys [J]. Journal of Applied Physics, 2002, 91(10): 7358−7360.

[6] CULLEN J R, CLARK A E, WUN-FOGLE M, RESTORFF J B, LOGRASSO T A. Magnetoelasticity of Fe−Ga and Fe−Al alloys [J]. Journal of Magnetism and Magnetic Materials, 2001, 226−330: 948−949.

[7] LOGRASSO T A, ROSS A R, SCHLAGEL D L, CLARK A E, WUN-FOGLE M. Structural transformations in quenched Fe−Ga alloys [J]. Journal of Alloys and Compounds, 2003, 350(1−2): 95−101.

[8] BORMIO-NUNES C, SATO TURTELLI R, GRÖSSINGER R, MÜLLER H, SASSIK H. Magnetostriction of melt-spun $Fe_{85}Ga_{15}$, $Fe_{78}Ni_7Ga_{15}$ and $Fe_{78}Co_7Ga_{15}$ stacked ribbon samples [J]. Journal of Magnetism and Magnetic Materials, 2010, 322(9−12): 1605−1608.

[9] LIU Jing-hua, YI Fang, JIANG Cheng-bao. Structure and magnetostriction of the $Fe_{85}Ga_{15}$ wire [J]. Journal of Alloys and Compounds, 2009, 481(1−2): 57−59.

[10] LI J H, GAO X X, XIE J X, ZHU J, BAO X Q, YU R B. Large magnetostriction and structural characteristics of $Fe_{83}Ga_{17}$ wires [J]. Physica B: Condensed Matter, 2012, 407(8): 1186−1190.

[11] CLARK A E, WUN-FOGLE M, RESTORFF J B, LOGRASSO T A, CULLEN J R. Effect of quenching on the magnetostriction on $Fe_{1-x}Ga_x(0.13<x<0.21)$ [J]. IEEE Transactions on Magnetics, 2001, 37(4): 2678−2680.

[12] PASCARELLI S, RUFFONI M, SATO TURTELLI R, KUBEL F, GRÖSSINGER R. Local structure in magnetostrictive melt-spun $Fe_{80}Ga_{20}$ alloys [J]. Physical Review B, 2008, 77(18): 184406-1−184406-8.

[13] MEHMOOD N, VLASÁK G, KUBEL F, TURTELLI R, GRÖSSINGER R, KRIEGISCH M, SASSIK H, SVEC P. Magnetostriction of rapidly quenched Fe−*X* (*X*=Al, Ga) ribbons as function of the quenching rate [J]. IEEE Transactions on Magnetics, 2009, 45(10): 4128−4131.

[14] HU Yong, DING Yu-tian, ZHANG Yan-long, WANG Guo-bin, ZHOU Zhi-guang. Magnetostriction and structural characterization of Fe−Ga bulk alloy prepared by copper mold casting [J]. Transactions of Nonferrous Metals Society of China, 2012, 22(9): 2146−2152.

[15] LI Chuan, LIU Jing-hua, JIANG Cheng-bao. Effect of the growth velocity on microstructure, orientation, and magnetostriction in $Fe_{81}Ga_{19}$ alloy [J]. Metallurgical and Materials Transactions A, 2012, 43(12): 4514−4519.

[16] RAVEL Á, NEWVILLE M. ATHENA, ARTEMIS, HEPHAESTUS: data analysis for X-ray absorption spectroscopy using IFEFFIT [J]. Journal of Synchrotron Radiation, 2005, 12(4): 537−541.

[17] LEE P, CITRIN P, EISENBERGER P T, KINCAID B. Extended X-ray absorption fine structure—Its strengths and limitations as a

structural tool [J]. Reviews of Modern Physics, 1981, 53(4): 769−806.

[18] CAO H, GEHRING P, DEVREUGD C, RODRIGUEZ-RIVERA J, LI J, VIEHLAND D. Role of nanoscale precipitates on the enhanced magnetostriction of heat-treated galfenol ($Fe_{1-x}Ga_x$) alloys [J]. Physical Review Letters, 2009, 102(12): 127201-1−127201-4.

[19] KUMAGAI A, FUJITA A, FUKAMICHI K, OIKAWA K, KAINUMA R, ISHIDA K. Magnetocrystalline anisotropy and magnetostriction in ordered and disordered Fe−Ga single crystals [J]. Journal of Magnetism and Magnetic Materials, 2004, 272−276: 2060−2061.

[20] ZHANG Jing-jing, MA Tian-yu, YAN Mi. Effect of heat treatment on structure, magnetization and magnetostriction of $Fe_{81}Ga_{19}$ melt-spun ribbons [J]. Physica B: Condensed Matter, 2009, 404(21): 4155−4158.

[21] ZHOU Z, WANG Y, GAO J, KOLBE M. Microstructure of rapidly solidified Cu−25wt.%Cr alloys [J]. Materials Science and Engineering A, 2005, 398(1): 318−322.

[22] CULLEN J, ZHAO P, WUTTIG M. Anisotropy of crystalline ferromagnets with defects [J]. Journal of Applied Physics, 2007, 101(12): 123922-1−123922-4.

[23] SEO Y, LEE B, KIM Y, LEE K. Grain size effects on magnetomechanical damping properties of ferromagnetic Fe−5wt.% Al alloy [J]. Materials Science and Engineering A, 2006, 431(1−2): 80−85.

不同甩速制备的 $Fe_{77}Ga_{23}$ 甩带合金的磁致伸缩性能和显微组织

刘 昊[1]，王海欧[1]，曹梦雄[1]，谭伟石[1]，时阳光[2]，徐 锋[3]，贾全杰[4]，黄宇营[5]

1. 南京理工大学 理学院应用物理系，软化学与功能材料教育部重点实验室，南京 210094；
2. 南京航空航天大学 理学院应用物理系，南京 211106；
3．南京理工大学 材料科学与工程学院，南京 210094；
4. 中国科学院 高能物理研究所，北京 100039；
5. 中国科学院 上海应用物理研究所，上海 201800

摘 要：采用 7、12.5 和 25 m/s 的甩速制备 $Fe_{77}Ga_{23}$ 甩带合金(分别命名为样品 S_7，$S_{12.5}$ 和 S_{25})。高分辨 X 射线衍射谱表明：样品的主体相均为 A_2 相，在样品 $S_{12.5}$ 和 S_{25} 中观测到了修正 DO_3 相，同时发现样品 S_{25} 具有较强的(100)织构。Ga 的 K 边扩展边 X 射线吸收精细结构谱表明：随着甩速的增大，Ga 的次近邻 Ga 原子个数减少并伴随着次近邻 Ga—Ga 键长收缩。在所有样品中均未发现 Ga 原子团簇。研究表明：样品 S_7 中短程有序的富 Ga 相和大的局域应变对样品 S_7 的磁致伸缩性能并无明显影响，(100)织构和修正 DO_3 相共同促进了 $Fe_{77}Ga_{23}$ 甩带合金的磁致伸缩性能。

关键词：磁致伸缩；织构；修正 DO_3 相；$Fe_{77}Ga_{23}$ 甩带合金

(Edited by Chao WANG)